Polyesters from renewable 1,4:3,6-dianhydrohexitols for food packaging: Synthesis, thermal, mechanical and barrier properties

Xuelian Liu, Nicolas Desilles, Laurent Lebrun

Version of Record: https://www.sciencedirect.com/science/article/pii/S0014305720310077
Manuscript_45b2d6625003f81971953438a66ea797

Polyesters from renewable 1,4:3,6-dianhydrohexitols for food packaging: synthesis, thermal, mechanical and barrier properties

Xuelian Liu, Nicolas Desilles, Laurent Lebrun*

Normandie Univ, UNIROUEN, INSA Rouen Normandie, CNRS UMR6270, PBS, 76000 Rouen, France

* Corresponding author. Tel: +33 2 35 14 67 02. Fax: +33 2 35 14 67 04.

E-mail address: laurent.lebrun@univ-rouen.fr (L. Lebrun).

Abstract

In the present work, biodegradable polyesters were synthesized by polycondensation reactions of renewable 1,4:3,6-dianhydrohexitols (isosorbide, IS; isomannide, IM) with aliphatic dicarboxylic acid chlorides containing 4, 6 and 10 carbons (namely, C4, C6 and C10) using a non-solvent method. All polyesters showed a thermal stability up to 320 °C and the glass transition temperature varied from 0 to 68 °C. Films were prepared by hot pressing. The semi-crystalline ISC10 and IMC10 films showed good mechanical properties with Young's modulus E =127±20 MPa, E =125±10 MPa and elongation at break ε = 19±5%, ε = 16±3%, respectively. The water sorption (liquid and vapor) of films was slow and low due to their crystalline micro-structures. The films were strongly barrier for gases with permeability coefficients P_{N_2} = 0.09, P_{O_2} = 0.26, P_{CO_2} = 1.32 barrer for ISC10, and P_{N_2} = 0.18, P_{O_2} = 0.46, P_{CO_2} = 2.04 barrer for IMC10. Furthermore, the high CO_2 and O_2 selectivity coefficients of ISC10 (α_{CO_2/O_2} = 5.1) and IMC10 (α_{CO_2/O_2} = 4.4) were favorable for the fruits and vegetables preservation. ISC10 film showed a better quality for food packaging in terms of mechanical and gas permeation properties compared to IMC10 film. A detailed discussion of the relationships between microstructures and sorption/permeation properties was conducted.

Keywords: Bio-based polyesters; Semicrystalline films; Food packaging; Barrier properties; Structure-property relationship.

Introduction

Food packaging is an indispensable part of our daily lives, and its demand is still growing. Traditionally, food packaging plastics (PET, PP, PE) are prepared from petroleum. The increase use of this limited resource aggravated global warming. At the Paris climate conference (COP21) in December 2015, 195 countries adopted the first-ever universal, legally binding global climate deal. The agreement set out a universal action plan to limit global warming with the reorientation of the world economy towards a low carbon model. Among the proposed solutions, one would be to use natural, biodegradable materials made from renewable resources. According to statistics, the total market of biodegradable materials exceeded $1.1 billion in 2018 and is predicted to reach $1.7 billion in 2023, where food packaging and disposable tableware are the main driving forces [1]. The biopolymers currently used for industrial applications are poly(hydroxyalkanoate) (PHA) and poly(lactic acid) (PLA) but they often show low mechanical properties and thermal stability [2,3]. Thus, the preparation of new bio-based materials, semi-crystalline, with better mechanical and thermal properties than PLA and PHA is scientific, industrial and environmental challenges. The progresses in polymer science suggest to synthesize new bio-based polymers [4–7]. However, thermal, mechanical and biodegradable properties of these new polymers must be studied before considering the replacement of conventional polymers [8–10]. Naturally bifunctional and thermally stable monomers can be extracted from biomass. Among them, 1,4:3,6-dianhydrohexitols (isosorbide, IS; isomannide, IM; isoidide, II) derived from cereals can be used as monomers for synthesizing bio-based polyesters [11–15].

As natural, chiral, rigid and non-toxic chemicals with functionalities, 1,4:3,6-dianhydrohexitols attracted extensive interests in medical [16–21], chemical [22–26] and polymer sciences [11,27–29]. Since 1984, 1,4:3,6-dianhydrohexitols have been used to synthesize polyesters but only IS and IM were widely studied due to their commercial availability [30]. Numerous patents and large amount of research articles based on these platforms, especially isosorbide, have been published. Within only the recent ten years, four review articles have covered all aspects of isosorbide chemistry [11,15,27,31]. In polymer chemistry, the sustainable, high-temperature resistant and biodegradable polymers based on 1,4:3,6-dianhydrohexitols are the ongoing hot topics. The combination of isosorbide with other renewable chemicals, such as aliphatic diacids and 2,5-furandicarboxylic acid to prepare thermosets have been reported as well [32–35]. The industry has also developed commercial polycarbonates and polyesters based on isosorbide, such as Polysorb® PSA, LP and PA,

produced by Roquette [36]. However, the low reactivity of the secondary alcohols of IS and IM made it hard to obtain high molar mass polyesters. Chemical modifications to increase the reactivity of IS were tried but with complicated and costly steps [37]. General ways to obtain aliphatic polyesters by reacting a wide range of dicarboxylic acids, from 2 to 36 carbons, with IS or IM were presented [38,39]. These polyesters were proved to be biodegradable [40,41] and compatible for using in implant biomedical materials [42]. The tetrahydropyran rings were found to increase the chains rigidity and then the T_g [6]. Multiple isosorbide-derived monomers for the synthesis of high thermal performance polyesters which could be used for hot-fill containers were also overviewed [28]. More recently, the effects of stereoisomerism of IS or IM and chain length of dicarboxylic acid units on the crystallization of the polyesters were investigated [43,44]. However, there is no investigation on gas and water permeation which is crucial to maintain the food shelf-life in packaging [45,46].

In this work, bio-based polyesters were prepared by reacting IS or IM with aliphatic diacid chlorides (succinyl, adipoyl and sebacoyl chlorides) according to the melt polycondensation previously published by Okada et al.[41]. These polyesters were proved to be biodegradable [40,41]. The originality of this work was to prepare films and investigate their gas and water sorption/permeation properties, which are crucial for food packaging applications. Relationships between microstructures and sorption/permeation properties were established.

1 Experimental

1.1 Chemicals

Isosorbide (98%), isomannide (95%), succinyl chloride (95%), adipoyl chloride (98%), sebacoyl chloride (≥95%), ethylene glycol (> 99%) and decane (> 99%) were purchased from Sigma-Aldrich. Dichloromethane (reagent grade) was provided by Fisher Scientific. Methanol (reagent grade) was supplied by VWR. All reagents were used as received without further purification.

1.2 Synthesis of the polyesters

IS (or IM) (60 mmol) was weighed into a 100 mL three-necked round-bottomed flask equipped with a mechanical stirrer and dipped into an oil bath (80 and 95 °C for IS and IM, respectively). Liquid succinyl chloride (60 mmol) was added when isosorbide was fully molten. The temperature was increased to 160 °C when the hydrogen chloride release

decreased, and the mixture was kept under normal pressure for 6 h under N_2 atmosphere. Then, reduced pressure was applied: 50 mbar for 2 h, then 0.1 mbar for 15 h. After cooling to room temperature, the media was dissolved in dichloromethane (50 mL) and the polyester was precipitated in methanol (500 mL). The polymers were purified by 3 times repeated dissolution precipitation. Finally, they were dried for 2 days at 40 °C under reduced pressure. All the polyesters were synthesized by the same way.

1.3 Preparation of the films

The films were processed by compression molding (thickness around 150 µm) using a hot press (Scamex, France) according to the following conditions: 5 min under 50 bars at different temperatures (given in Figure 5). The films were then stored at room temperature in a desiccator with P_2O_5 under room temperature for a constant time (60 days after hot pressing).

1.4 Characterization of the polymers

1.4.1 Polymer structure

The chemical structures were confirmed by FT-IR (VERTEX 70 from Bruker) and by ^{1}H NMR (300 MHz Bruker spectrometer) at room temperature in $CDCl_3$. Chemical shifts (δ) were expressed in parts per million (ppm) and referenced to the internal deuterated solvents with tetramethylsilane as the internal standard.

1.4.2 Molar masses

The number average molar masses ($\overline{M_n}$) of the polyester samples were measured by steric exclusion chromatography (PL-GPC50 from Varian) at 27.5 °C. The solvent was dichloromethane and the analysis was carried out with PMMA calibration.

1.4.3 Thermogravimetric analysis (TGA)

The thermal decomposition of the polymers was investigated by TGA (TGA Q500 from TA Instruments) under nitrogen atmosphere. The sample (5-10 mg) was packed in a platinum pan and heated from 30 to 600 °C with a heating rate of 10 °C·min^{-1}.

1.4.4 Differential scanning calorimetry (DSC)

Differential Scanning Calorimetry measurements were performed with a DSC Q2000 from TA Instruments. The 5-10 mg samples were heated from -30 to 250 °C with 10 °C·min^{-1}

heating rate. T_g were measured at the mid-point, T_m at the peak maximum and ΔH_m thanks to the melting peak area.

1.5 Characterization of films

1.5.1 Wide angle X-ray diffraction (WAXD)

The crystal structures and crystallinity (χ_c) were evaluated using an X-Ray diffractometer D5000 from Bruker AXS. The radiation was λ_{Co} = 1.789 Å powered by a current of 40 mA and a voltage of 40 kV. The data were acquired on a scanning range $2\theta = 5°$-55° with a scanning speed of 0.004° s^{-1}. Intensity correction, crystallinity determination and peak separation were performed using PeakFit® software.

1.5.2 Polarized optical microscopy (POM)

Crystals in polyester films were observed using a DMLM Leica optical polarizing microscope. Image acquisition and analysis were performed with Archimed software.

1.5.3 Contact angle measurements

Contact angle (θ) and surface energy (γ) of films were determined at room temperature (23 °C), with three different liquids: water (MilliQ Millipore Water system), ethylene glycol and decane. The contact angle θ values were averaged from at least five measurements. The surface energy was calculated by Windrop++ Carrousel software according to Owens & Wendt method [47].

1.5.4 Mechanical properties

The tensile tests of polyester films were performed at room temperature (23 °C) using a ZwickRoell Z010 testing machine (TestXpert II-V3.5 software). The load cell was 500 N, the crosshead speed was 10 mm·min^{-1}, and the distance between the grips was 40 mm. The dumbbell shaped specimens were 1BB type according to the ISO 527-2:2014-04 standard. The tensile modulus (E) was determined in the linear part of the stress-strain curve. More than 10 tests were performed on each sample and the obtained values were averaged.

1.5.5 Liquid water sorption

The liquid water sorption measurements were performed at 25 °C by measuring the variation of the mass gain *vs* time of samples (initially dry) immersed in pure water (MilliQ Millipore Water system). Three measurements were carried out on each sample (A = 1 cm^2)

using a balance (precision 0.1 mg). The mass gain at t time (M_t) was calculated according to Eq. 1.

$$M_t = \frac{m_t - m_d}{m_d} \times 100 \qquad \text{(Eq. 1)}$$

with m_t the film mass at t time and m_d the dry film mass. The accuracy on M_t values was estimated lower than 10%.

1.5.6 Water vapor sorption

Water vapor sorption measurements were conducted with the automatic gravimetric dynamic vapour sorption DVS1 Advantage (Surface Measurement Systems Ltd) as previously described [48]. Different water vapor activity steps (a_w) ranging from 0 to 0.95 were applied at 25 °C on the film ($m \cong 15$ mg). At each step, the mass gain was measured as a function of time until the equilibrium was reached. The mass gain at equilibrium M_{eq} was calculated for each a_w according to Eq. 2, which allowed the plotting of water vapor sorption isotherms.

$$M_{eq} = \frac{m_{eq} - m_d}{m_d} \times 100 \qquad \text{(Eq. 2)}$$

with m_{eq} the film mass at equilibrium.

The accuracy on the values was lower than 4%. Kinetic data were extracted from the normalized mass gain M_t/M_{eq} *vs* reduced time ($t^{1/2}/L$), where M_t is the mass gain at time t (Eq.1). Reduced time was used to allow data comparisons independently of the film thickness L.

1.5.7 Water vapor permeation

The water vapor permeation measurements were performed using the home-made permeation cell previously described [49]. The experimental conditions were: $a_w \cong 0.20$, 0.50, 0.55 and 0.60, T = 25 °C, surface of the film $A = 3.6$ cm^2. The water vapor flux J through the film as a function of time t was measured. At steady state ($J = J_{st}$), the permeability coefficient P (expressed in g·m^{-1}·d^{-1}) was calculated from Eq. 3 [50]:

$$P = \frac{J_{st} \times L}{\Delta a_w} \qquad \text{(Eq. 3)}$$

where Δa_w is the difference in water activity across the film.

1.5.8 Gas permeation

Carbon dioxide (CO_2), oxygen (O_2) and nitrogen (N_2) permeation measurements were performed on films using the equipment previously described (25 °C, applied gas pressure 3 bar) [51]. The quantity of transferred gas Q through the film was detected versus time t (s). The permeability coefficient P (expressed in Barrer) was calculated according to Eq. 4:

$$P = \frac{L}{A\,\Delta P}\frac{dQ}{dt} \qquad \text{(Eq. 4)}$$

with L and A, thickness and surface (11.34 cm^2) of the film; Δp, pressure difference between the two sides of the film; dQ/dt, slope of the experimental curve at stationary state. The diffusion coefficient D ($cm^2 \cdot s^{-1}$) was calculated from the time-lag t_L value obtained from the extrapolation of the steady-state asymptote to the time axis [52]:

$$D = \frac{L^2}{6\,t_L} \qquad \text{(Eq. 5)}$$

2 Results and discussion

Six aliphatic polyesters were synthesized by using a non-solvent polymerization according to Figure 1. The polyesters were identified as follows: the first two letters corresponded to the dianhydrohexitol used (IS for isosorbide and IM for isomannide), followed by CX, where X represented the number of carbon atoms coming from the aliphatic chain of the diacid chloride.

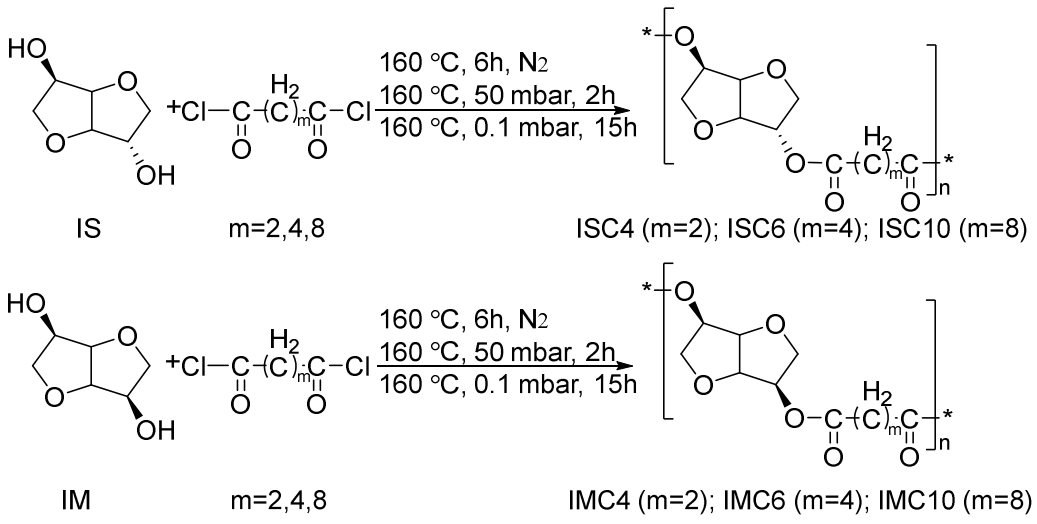

Figure 1 General route for the synthesis of aliphatic polyesters prepared from IS and IM with aliphatic dicarboxylic acid chlorides

2.1 Characterization of polymers

2.1.1 Structures

FT-IR spectra of the synthesized polyesters are given in Figure S1. Due to their similar chemical structures, all polyesters showed almost identical spectra. Taking ISC4 as an example (bottom of Figure S1), the double CH_2 stretching signals of the aliphatic chain appeared in the range from 2940 to 2870 cm^{-1} and the signal of ether cyclic bond in IS was at 1089 cm^{-1}. The presence of the ester group was proved by the pronounced C=O peak at 1730 cm^{-1} and the C-O double peaks at 1160 and 1140 cm^{-1}, which confirmed the successful synthesis.

The chemical structures of the polyesters were also characterized by ^1H NMR. The spectra of ISC10 and IMC10 were shown in Figure 2a and Figure 2b respectively, and the others were given in supplementary material (Figure S2). In Figure 2a, the proton signals in the range from 5.22 to 3.68 ppm (8H) corresponded to isosorbide and the signals at 2.33 (4H), 1.61 (4H) and 1.29 (8H) ppm were attributed to methylene protons of sebacoyl chloride. Similarly in Figure 2b, the signals in the range from 3.67 to 5.19 ppm (8H) were ascribed to isomannide and the signals at 2.37 (4H), 1.63 (4H) and 1.30 (8H) ppm belonged to sebacoyl chloride. The exo hydroxyl group connected with the second carbon (C-2) of isosorbide ring induced the irregular structure of ISC10 that resulted in stereo differences between ISC10 and IMC10, which could explain the peaks splited more in ISC10 spectrum.

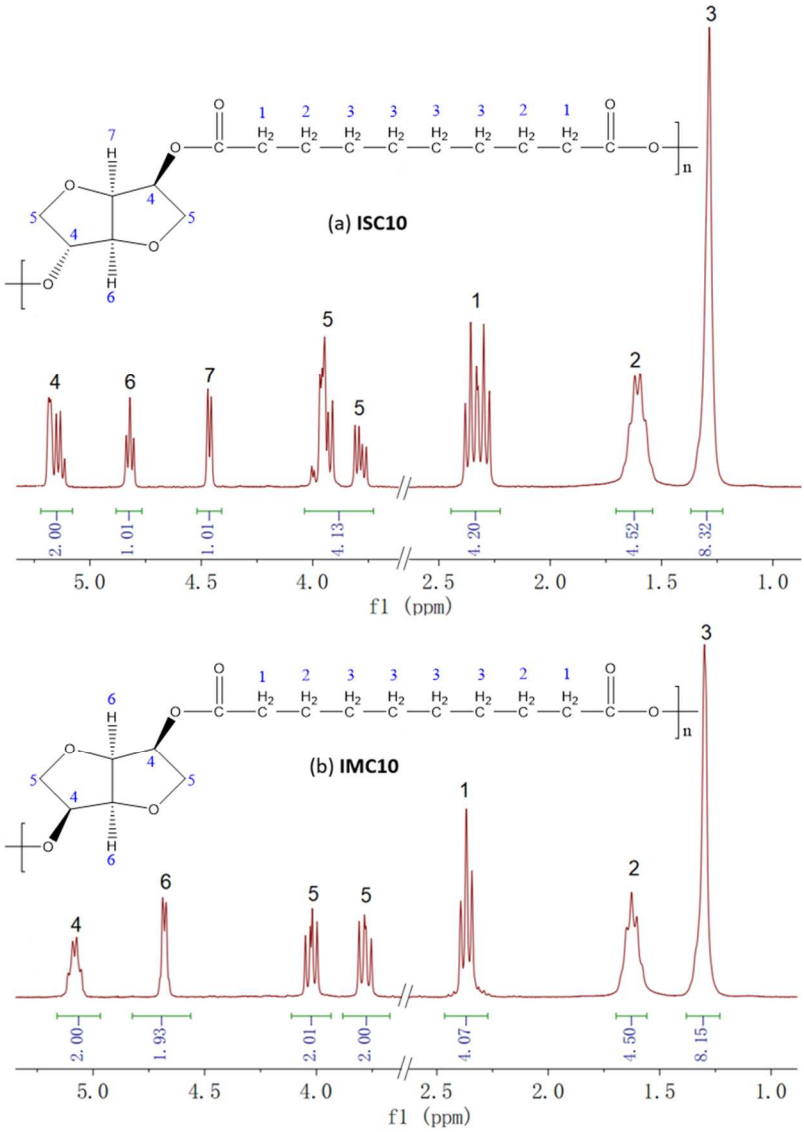

Figure 2 ^{1}H NMR spectra of (a) ISC10 and (b) IMC10

2.1.2 Molar masses

The polymer molar masses were determined by Steric Exclusion Chromatography (SEC) (Table 1). Except for IMC4, high yields were obtained and the molar masses ($\overline{M_n}$) of polyesters exceeded 10 000 g·mol^{-1}. The case of IMC4 can be ascribed to its high melting temperature around 173 °C (see section *2.1.4*), higher than the reaction temperature (160 °C), which limited the polycondensation reaction [43]. There is a general tendency that the molar mass increase with C atom number, probably due to the higher flexibility brought by the methylene units which would favor the motion of the growing chains in a very viscous bulk medium.

Table 1 The number average molar masses and dispersities of polyesters and yields of synthesis

Polyester	$\overline{M_n}$ [1)] (g·mol^{-1})	Đ [2)]	Yield (%)	Polyester	$\overline{M_n}$ [1)] (g·mol^{-1})	Đ [2)]	Yield (%)
ISC4	10 800	2.1	80	IMC4	4 300	1.8	62
ISC6	10 600	1.7	88	IMC6	15 500	2.5	85
ISC10	18 500	2.1	90	IMC10	19 000	2.0	89

[1)] SEC conducted in CH_2Cl_2 with PMMA standards. [2)] Dispersity

2.1.3 Thermal degradation

The thermal degradation of polyesters was investigated by thermal gravimetric analysis. The degradation curves were presented in Figure 3 and detailed data were recorded in Table S1. All polyesters showed a thermal stability up to 320 °C with a rapid decomposition around 400-450 °C. The degradation seemed to begin at higher temperatures when the length of the aliphatic diacid chain increased, with 5% weight loss temperature ($T_{5\%}$) values $T_{5\%}$(ISC4) < $T_{5\%}$(ISC6) < $T_{5\%}$(ISC10) and $T_{5\%}$(IMC4) < $T_{5\%}$(IMC6) < $T_{5\%}$(IMC10), which was probably due to the increased molar masses. Even if IMC10 showed the highest thermal stability, we cannot generally conclude that IM polyesters were more stable than IS homologues. It means that the diacid chain length has more influence on the thermal degradation than stereoisomerism. The results are consistent with literature values [42,43].

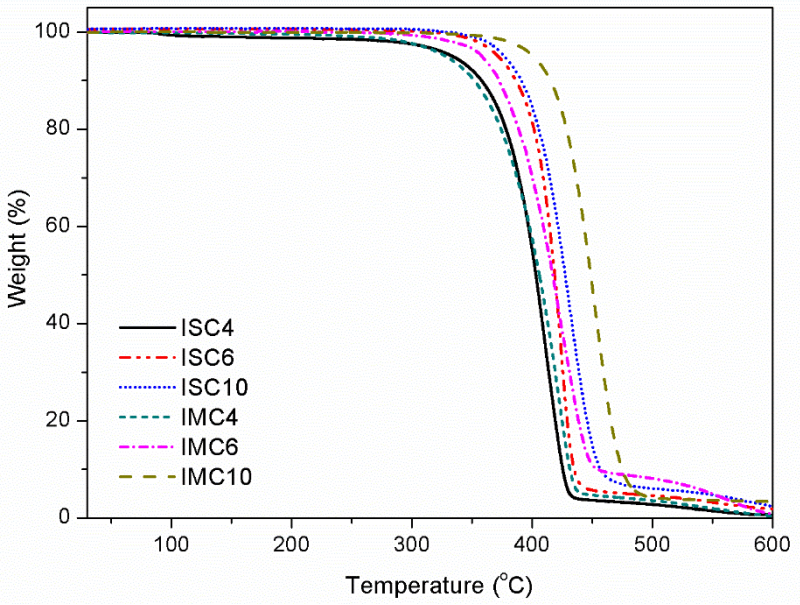

Figure 3 TGA curves of IS and IM polyesters

2.1.4 DSC

DSC measurements were carried out to determine the glass transition temperature (T_g) and the crystallization behavior of the polyesters. The first heating thermograms were presented in Figure 4 and detailed data were recorded in Table S2. It showed that only ISC10, IMC4 and IMC10 were semi-crystalline due to the presence of melting peaks. These melting peaks were complex, and could reveal not only melting / crystallization phenomena but more certainly crystalline polymorphism (as evidenced later from XRD patterns in Figure 7), as already observed in such polymers before [43]. However, the crystals cannot be obtained back upon cooling (Figure S3) probably due to the very slow crystallization rate. These results are in good agreement with those obtained by Marubayashi et al. [43] , except for IMC4, probably due to the low molar mass in our case. The T_g values decreased with the increase of the aliphatic carbon number, which is quite logical since more CH_2 in the chain induced more flexibility and free volume. The highest T_g (65 °C) was observed for IMC4 and the lowest (0 °C) for IMC10. For a given aliphatic chain, considering almost the same molar masses of ISC10 and IMC10, it seemed that IM and IS polyesters showed only slight difference on T_g value, but larger differences on crystallinity. It means that the endo-exo and endo-endo stereoscopic difference affected the crystallization rather than the chain relaxation [43].

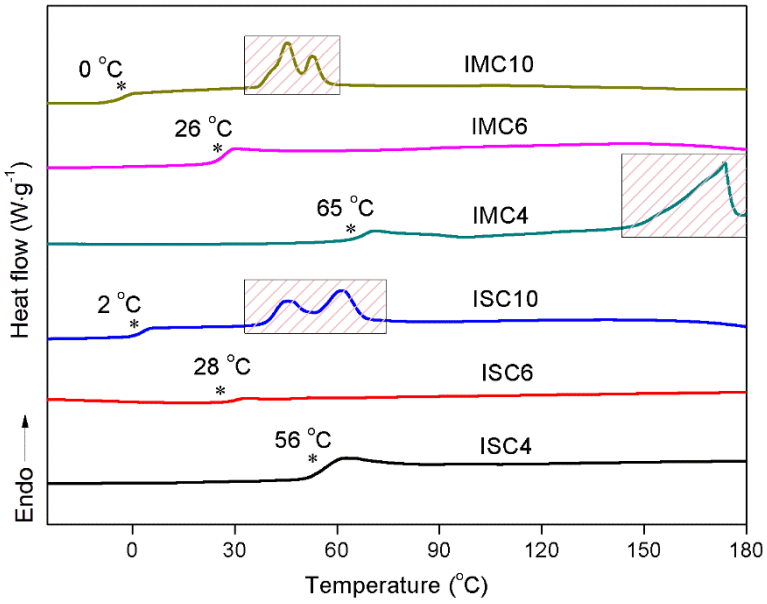

Figure 4 DSC first heating of IS and IM polyesters

2.2 *Characterization of polymer films*

2.2.1 *Preparation of polymer films*

The polymer films shown in Figure 5 were prepared by hot pressing under different temperatures depending on their thermal properties established by DSC. Since the obtained polymers could not recrystallize upon cooling, and the crystalline phase is well known to bring barrier properties, the films were sometimes prepared with partial melting. Unfortunately, ISC4, ISC6, IMC4 and IMC6 films appeared too brittle, which was probably due to their short methylene units and lower molar masses. Only ISC10 and IMC10 films with the highest molar masses and longer methylene units were flexible enough for the further experiments. IMC10 film was prepared at 45 °C (35 °C < T_m < 60 °C) and ISC10 film was prepared at 50 °C (35 °C < T_m < 72 °C). The yellow to brown color of films showed in Figure 5 came from polymerization but deepened after hot pressing, which was probably due to thermal oxidation. Since the crystals of ISC10 and IMC10 changed during time at the temperature range of 20-40 °C [43], the crystal structures should be confirmed before investigating the mechanical and barrier properties of polyester films.

ISC4 (100 °C) Brittle	ISC6 (60 °C) Brittle	ISC10 (50 °C) Flexible	IMC4 (190 °C) Brittle	IMC6 (60 °C) Brittle	IMC10 (45 °C) Flexible

Figure 5 IS and IM polyester films prepared by hot pressing

2.2.2 *DSC characterization of polyester films*

The melting behaviors of polyester films were investigated by DSC and compared to the corresponding polyesters in Figure 6. Both ISC10 and IMC10 films showed broad but less complex melting peaks compared to the corresponding polyesters. Furthermore, it seemed the initial melting temperature increased, which can correspond to an annealing process occurring during hot pressing and storage. The melting enthalpy (ΔH_m) of ISC10 film was 26.1 J·g^{-1}, which is higher than that of ISC10 (ΔH_m = 18.7 J·g^{-1}), but the melting enthalpy of IMC10 (ΔH_m = 15.9 J·g^{-1}) and IMC10 film (ΔH_m = 16.0 J·g^{-1}) were almost the same. Despite the partial melting during film making, and the fact that no crystallization was observed during cooling in DSC for both polyesters, the recrystallization could effectively happen due to the

annealing process during the hot pressing and the 60 days under room temperature storage. ISC10 film was more crystalline with a higher melting temperature than IMC10 film.

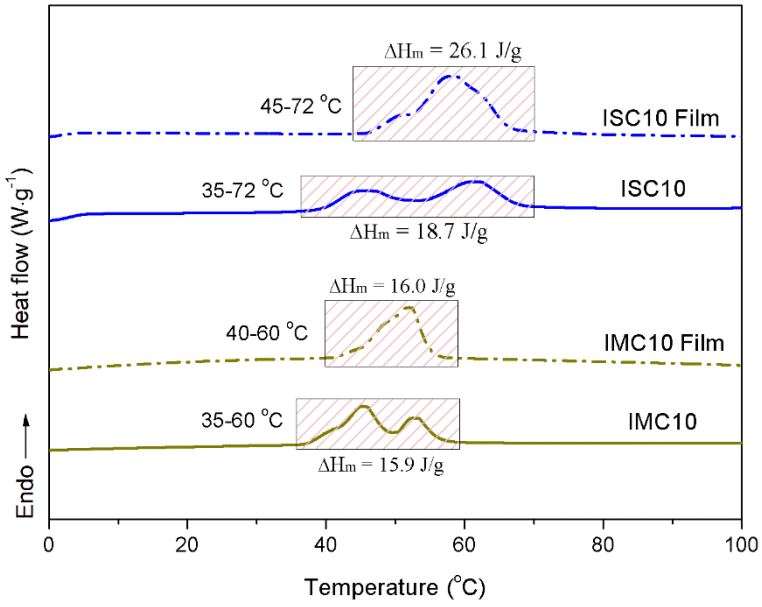

Figure 6 DSC first heating of ISC10 and IMC10 polyesters and films

2.2.3 XRD characterization of polyester films

Table 2 Crystallinity (χ_c) and *d*-spacing information for ISC10 film and IMC10 film

Polyester film	χ_c (%)	d_1 (nm)	d_2 (nm)
ISC10 film	36.3	1.60	0.46
IMC10 film	25.9	1.60	0.46

Figure 7 exhibited the XRD diffractograms of ISC10 film and IMC10 film. The crystallinity (χ_c) and *d*-spacing were recorded in Table 2. Two obvious diffraction peaks located at 2θ~6.5° and 2θ~22.5° corresponded to d_1 = 1.60 nm and d_2 = 0.46 nm respectively for both polyester films. This result was consistent with Marubayashi et al. [43]. The *d*-spacing d_1 corresponded to the spacing parallel to the chain direction and d_2 was that perpendicular to the chain direction (chain-chain packing). The crystallinity of ISC10 film (χ_c = 36.3%) is higher than IMC10 film (χ_c = 25.9%): ISC10 is more crystallized by chain-chain packing than IMC10. Besides, the diffractometric patterns show scattering peaks at very low 2θ values (5-10°) which can be related to liquid crystal regions as reported by Ding et al. [53].

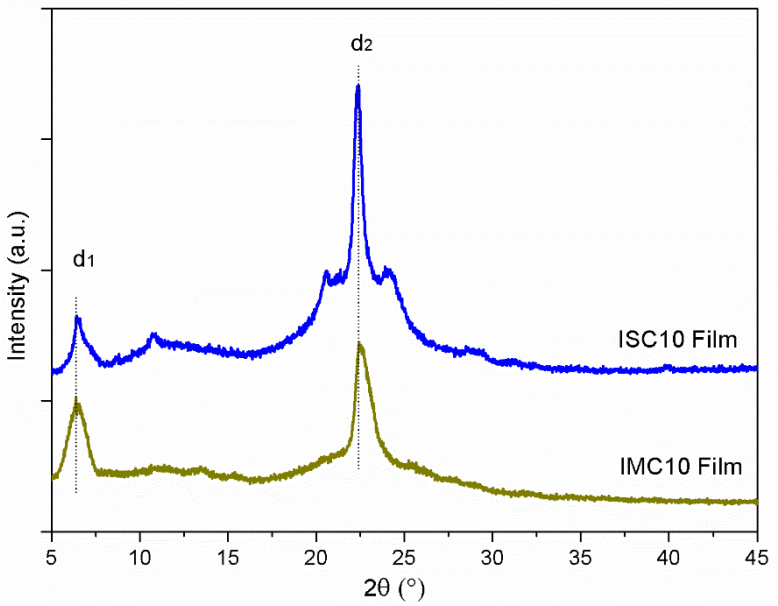

Figure 7 XRD spectra of ISC10 and IMC10 polyester films

2.2.4 Microscopy of polyester films

Polyester films microscopy images shown in Figure 8 proved that ISC10 film contained larger but less homogeneous crystals than IMC10. The ISC10 film microstructure well corresponded to a broader and higher melting temperature observed by DSC, compared to IMC10. It evidenced that the endo-exo stereoscopic configuration in IS polymer chains were more inclined to crystallize in larger size than the endo-endo stereoscopic configuration in the IM polymer chains [43]: the IS chains are more readily to crystallize by chain-chain interactions (chain-chain packing). Moreover, the textures evidenced by POM images are typical of liquid crystal phase [53–55].

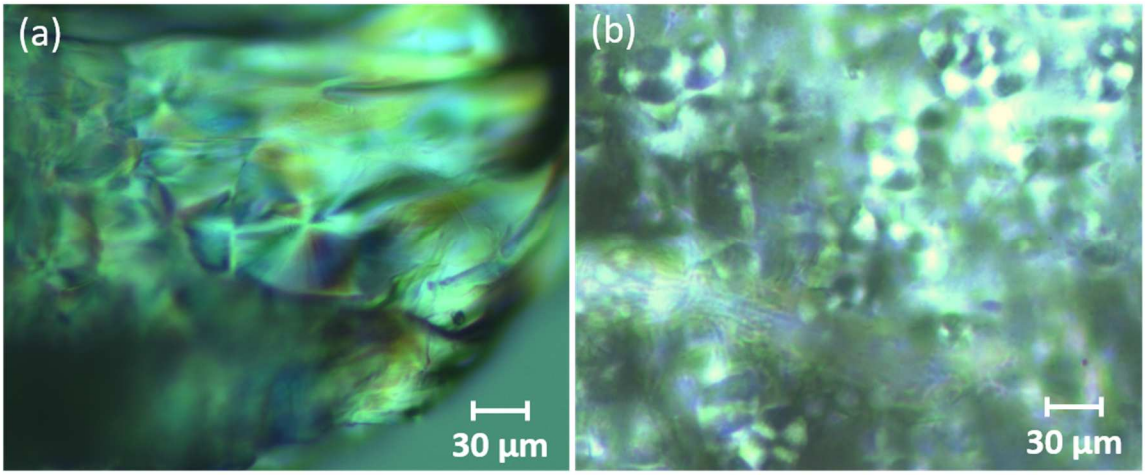

Figure 8 Microscopy images of ISC10 film (a) and IMC10 film (b)

2.2.5 *Mechanical properties*

The mechanical properties of ISC10 and IMC10 were gathered in Table 3. ISC10 had a better resistance to stretch than IMC10. The Young's modulus values of ISC10 and IMC10 were similar (127 ± 20 MPa and 125 ± 10 MPa respectively). Comparing the ultimate tensile strength and elongation at break, ISC10 (σ_b= 4.2 ± 0.8 MPa, ε_b = 19 ± 5 %) seemed tougher than IMC10 (σ_b= 1.0 ± 0.2 MPa, ε_b = 16 ± 3 %). Since their molar masses and T_g were very similar, it seemed that the higher crystallinity and larger crystal size of ISC10 brought more resistance at break. Both ISC10 and IMC10 had more toughness than PLA (elongation at break less than 10%) [56]. However, our ISC10 films were more rigid and more brittle than those prepared by Park et al. [42] (E = 53 MPa and σ_b = 10.5 MPa). The differences may be due to the solvent casting technique used by Park et al. to prepare their films. With this technique, solvent molecules can be retained and plasticize the film.

Table 3 Mechanical properties of ISC10 and IMC10 polyester films

Polyester film	E (MPa)	σ_b (MPa)	ε_b (%)
ISC10	127 ± 20	4.2 ± 0.8	19 ± 5
IMC10	125 ±10	1.0 ± 0.2	16 ± 3

E, Young's modulus; σ_b, Stress at break; ε_b, Strain at break.

2.2.6 *Contact angle measurements*

The surface energy (with dispersity and polar parts) and water contact angle values of polyester films were presented in Table 4. The surface energy values for ISC10 (31.0 $mN{\cdot}m^{-1}$) and IMC10 (29.6 $mN{\cdot}m^{-1}$) were similar. The water contact angle values, 85 ± 1.0° for ISC10 and 83 ± 0.5° for IMC10, highlighted the hydrophobicity of the films. The results showed almost no difference between ISC10 and IMC10, indicating that the surfaces properties of the films were not influenced by the stereoisomerism of IS and IM. The water contact angles of ISC10 and IMC10 were lower than the common used packaging materials PE (120 ± 0.1°) [57], PP (97 ± 0.4°) [58], but comparable to semi-crystalline polyesters like PET (83.8 ± 1.0°) [59] and PLA (80.0 ± 0.1° and 73.0 ± 2.0°) [2,60].

Table 4 Surface energies and contact angles of ISC10 and IMC10 polyester films

Polyester film	γ^t ($mN{\cdot}m^{-1}$)	γ^d ($mN{\cdot}m^{-1}$)	γ^p ($mN{\cdot}m^{-1}$)	θ (°)
ISC10	31.0	26.1	4.9	85.0 ± 1.0
IMC10	29.6	24.1	5.4	83.0 ± 0.5

γ^t, Total surface energy with the dispersive (γ^d) and polar (γ^p) parts; θ, water contact angle.

2.2.7 *Liquid water sorption and water vapor sorption*

Figure 9 showed that the sorption of liquid water is low whatever the sample. This behavior can be explained by the semi-crystalline micro-structures of the polyester films. The equilibrium was earlier reached (before 2800 min) for IMC10 than for ISC10 (after 2800 min), which meant IMC10 proceeded a quicker dissolution-diffusion process than ISC10. The sorption was less pronounced for ISC10 (M_t at equilibrium = M_{eq} = 0.55 ± 0.05 %) than for IMC10 (M_{eq} = 1.03 ± 0.04 %). This is due to the bigger size crystals and the higher crystallinity of ISC10, which bring more compact structure favorable for water barrier properties.

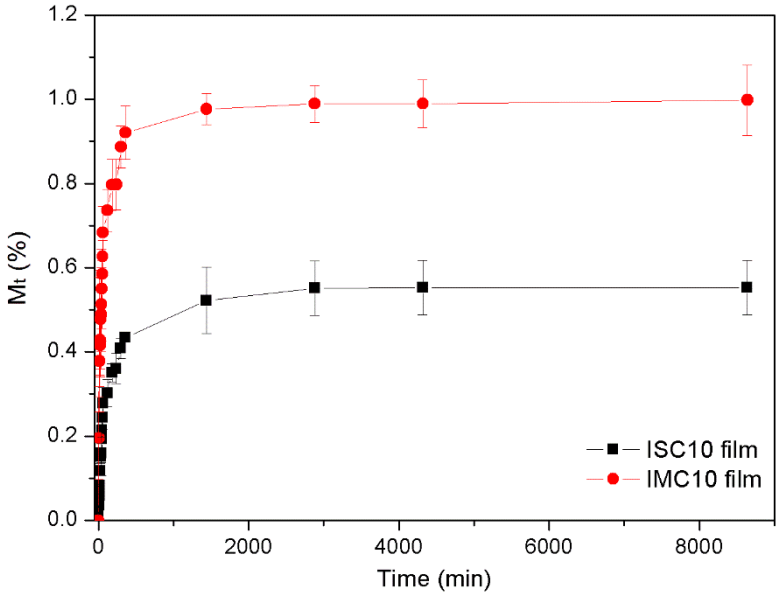

Figure 9 Liquid water sorption of ISC10 and IMC10 films

As observed before for liquid water sorption, water vapor sorption was less for ISC10 than for IMC10 (*e.g.* M_{eq} = 0.58 % and M_{eq} = 1.08 % at water activity a_w = 0.95, respectively). Both ISC10 and IMC10 showed a constant sorption of water vapor at the lower a_w then a larger increase (Figure 10a). The linear isotherm describes a Henry's type process corresponding to a random absorption (dissolution) and then a diffusion of the water molecules inside the film. This isotherm corresponded to the sorption of the water molecules in the free volume of the polymer. The slope of the straight line corresponds to the solubility coefficient S of water vapor in the film. ISC10 showed a constant sorption until a_w = 0.8 (S = 5.3 x 10^{-3} g_{H_2O}/g_{pol}) and IMC10 until a_w = 0.5 (S = 8.0 x 10^{-3} g_{H_2O}/g_{pol}). The convex part of the curve highlighted an adsorption of water molecules with formation of aggregates, which

induced a larger swelling of the film. This accumulation of water molecules took place in the free volume of the amorphous phase, which means there are more free volume in IMC10 than in ISC10 films.

The kinetics of water sorption were presented by the normalized gain of mass (M_t/M_{eq}) *vs* reduced time ($t^{1/2}\ L^{-1}$) for different vapor activities (Figure 10b). It is obvious that IMC10 showed a quicker dissolution-diffusion process of water vapor than ISC10, which agreed with the liquid water sorption. A slowing-down process was observed at high a_w. The detailed sorption kinetics data were interpreted in terms of rate of diffusion of water molecules by considering t_r time to reach the equilibrium of sorption. For a short time (when $M_t/M_{eq} < 0.2$), the slope (k_1) of the linear regression of the curves $(M_t/M_{eq})^2 = f(t - t_r)$ allowed the calculation of water diffusion coefficient D_1: $D_1 = k_1\ \pi\ L^2\ /\ 16$. For a longer time ($M_t\ /\ M_{eq} > 0.7$), the slope k_2 of the linear regression of the curve ($\ln (1 - M_t/M_{eq}) = f(t)$) allowed the determination of the water diffusion coefficient D_2: $D_2 = k_2\ L^2\ /\ \alpha_1$ ($\alpha_1 = 2.40483$) [48]. The changes of D_1 and D_2 for IMC10 and ISC10 as a function of a_w were given Figure 10c. The variation of the D_1 and D_2 values are in agreement with the isotherm. The D_1 values appeared higher than D_2 probably due to the aggregation of the water molecules during the sorption, which makes them less mobile. The D values were constant on large water activity range. This constant diffusion of the water molecules inside the film was in accordance with the Henry's behavior previously observed on the isotherms. The decrease of D_1 and D_2 coefficients at high a_w (> 0.8) could be explained by the largest aggregation of water molecules. D_1 and D_2 values were higher for IMC10 than for ISC10, which is consistent with the kinetics. The larger size of the crystal structure and the higher crystallinity previously observed in ISC10 can explain this result. The low permeable crystal structures that stand in the way of the water molecules increased the tortuosity of the diffusion path, and consequently decreased D.

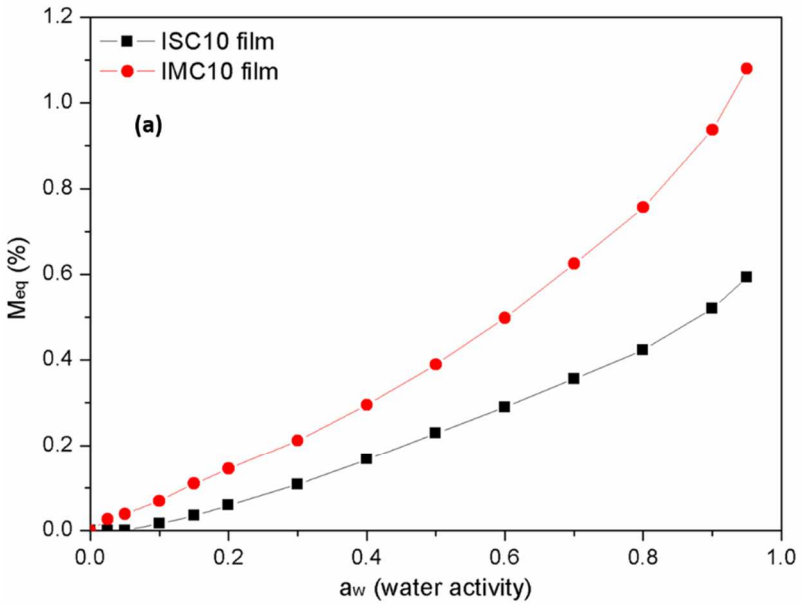
ISC10 film
IMC10 film
(a)
Meq (%)
aw (water activity)

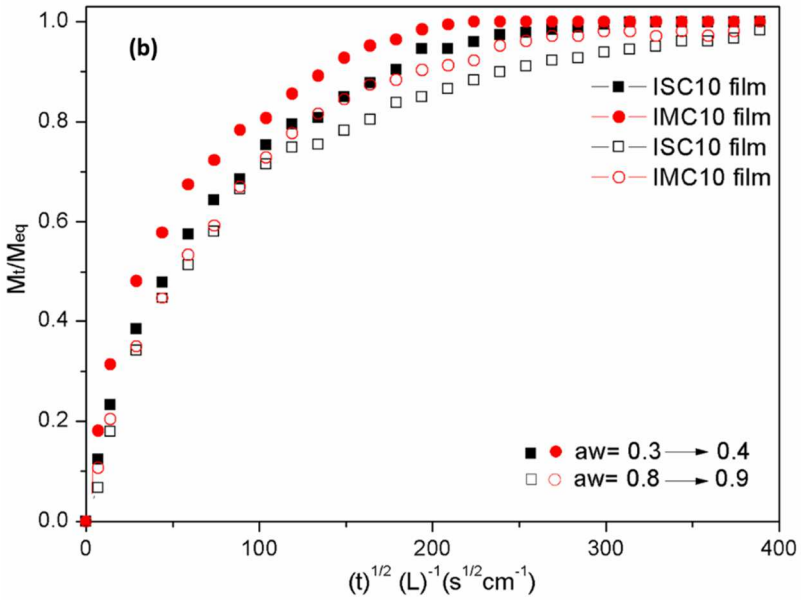
(b)
ISC10 film
IMC10 film
ISC10 film
IMC10 film
aw= 0.3 → 0.4
aw= 0.8 → 0.9
Mt/Meq
(t)1/2 (L)-1(s1/2cm-1)

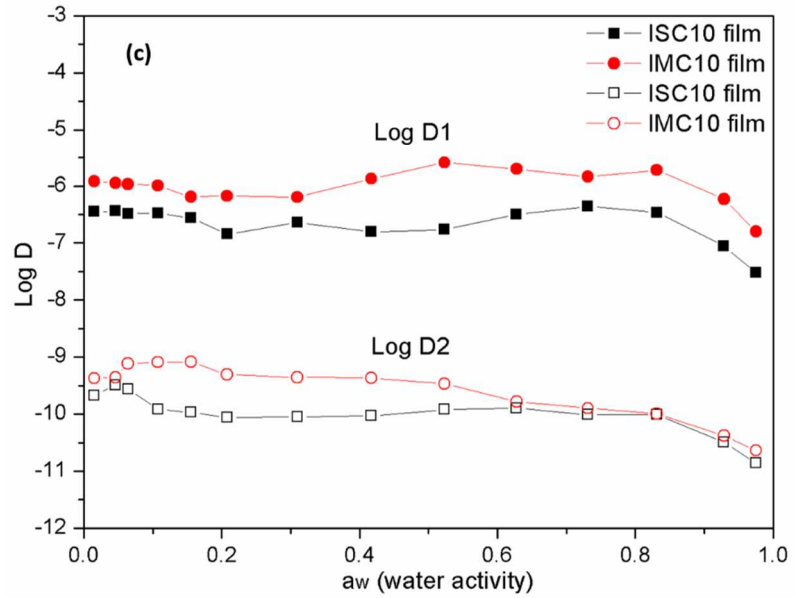
(c)
ISC10 film
IMC10 film
ISC10 film
IMC10 film
Log D1
Log D2
Log D
aw (water activity)

Figure 10 Water vapor sorption of ISC10 and IMC10 films: (a) sorption isotherm (b) sorption kinetics (c) diffusion kinetics

2.2.8 Water vapor permeation

Water vapor permeability coefficients (*P*) of ISC10 and IMC10 are given Table 5 for different water activities. ISC10 film showed the lowest *P* values whatever a_w (*e.g.* P = 1.55 $g \cdot m^{-1} \cdot d^{-1}$and P = 2.81 $g \cdot m^{-1} \cdot d^{-1}$at $a_w \cong 0.5$ for ISC10 and IMC10, respectively). These results are in accordance with those previously obtained by sorption measurements. The lowest *P* values obtained for ISC10 could be related to the lowest solubility coefficients *S* and diffusion coefficients *D* ($P = D \times S$). Considering the same elements composition of ISC10 and IMC10, it could be concluded that the micro-structure of the ISC10 film brought more barrier for water molecules. ISC10 showed a comparable water vapor barrier referred to PLA (25 ºC, a_w=0.5, P= 1.39-1.63 $g \cdot m^{-1} \cdot d^{-1}$) [61]. However, ISC10 was less barrier than PET (21 ºC, a_w=0.4, P= 0.47 $g \cdot m^{-1} \cdot d^{-1}$) [62], which is probably due to its low glass transition temperature and the presence of the "Oxygen" in the IS molecular ring in the amorphous phase.

Table 5 Water permeation coefficient (*P*) of ISC10 and IMC10 films at different water activities (a_w).

Polyester film	*a*w	*P* ($g \cdot m^{-1} \cdot d^{-1}$)
ISC10	0.25	0.04
	0.48	1.55
	0.55	3.78
	0.65	5.10
IMC10	0.19	0.33
	0.49	2.81
	0.55	5.61
	0.60	5.95

2.2.9 Gas permeation measurements

Table 6 presented the values of permeability (*P*) and diffusion (*D*) coefficients of ISC10 and IMC10 films. It could be easily observed that both ISC10 and IMC10 showed low gas permeability, which is probably due to the presence of crystals and liquid crystal regions, which are strongly barrier to gases [63–65]. ISC10 showed higher barrier properties than IMC10 due to its higher crystallinity, as previously explained for water. The permeability coefficients *P* of ISC10 for N_2, O_2 and CO_2 were 0.09, 0.26 and 1.32 barrer, respectively, which is similar to PLA (P_{O_2}= 0.16 barrer, P_{CO_2} = 1.27 barrer) [66]. ISC10 and IMC10

appeared both more barrier to gases than the commonly used food packaging material PE (P_{O_2}=3.2 barrer, P_{CO_2}=11.7 barrer) [67] but less barrier than PET (P_{N_2} = 0.008 barrer, P_{O_2}= 0.03 barrer, P_{CO_2}= 0.15 barrer) [68] and semi-crystalline PEF (P_{O_2}= 0.004~0.006 barrer, P_{CO_2}= 0.01~0.02 barrer) [69]. To optimize a packaging, the selectivity [70] between CO_2 and O_2 (α_{CO_2/O_2}) should be controlled because the respiration rate of fruits and vegetables should be slowed down. Thus, it is necessary to limit the oxygen content while increasing the concentration of carbon dioxide to keep the vegetables fresh as long as possible[71]. However, the packaging must be a little permeable to oxygen because a too low concentration of oxygen triggers an anaerobic breathing process which induces bad taste and bad odors to vegetables, and then decrease their shelf-life. The selectivity coefficient α_{CO_2/O_2} for ISC10 (α_{CO_2/O_2}= 5.1) was comparable to petroleum-based common food packaging polyester PET (α_{CO_2/O_2}= 5.0) [68], but larger than for IMC10 (α_{CO_2/O_2}= 4.4), bio-based potential food packaging polyester PLA (α_{CO_2/O_2}= 1.0~2.0) [72] and PEF ($\alpha_{CO_2/O_2} \cong$ 3) [69], which indicated that ISC10 is more favorable for the fruits and vegetables preservation.

The diffusion coefficient *D* was lower for ISC10 than for IMC10 whatever the gas (Table 6). These results were consistent with those obtained with water: the higher crystallinity and bigger crystals in ISC10 increased the tortuosity of the diffusion pathway, and also meant less free volume and less exposure of oxygen atoms in the ISC10 film, which could explain the lowest solubility to O_2 and CO_2 gases ($S=P/D$).

Table 6 Gas permeation (*P*) and diffusion (*D*) coefficients of ISC10 and IMC10 films

Polyester film	N_2		O_2		CO_2	
	P	*D* x 10^6	*P*	*D* x 10^7	*P*	*D* x 10^8
ISC10	0.09	1.26	0.26	2.78	1.32	1.98
IMC10	0.18	2.50	0.46	3.86	2.04	2.54

P expressed in barrer (1 barrer = 10^{-10} cm^3 STP·cm·cm^{-2}·s^{-1}·$cmHg^{-1}$), *D* expressed in cm^2·s^{-1}.

2.2.10 Relationship between microstructure and permeation properties

As discussed before, the barrier properties of ISC10 and IMC10 may result not only from their semi-crystalline nature but also from the presence of liquid crystal regions, since these polymers contain rigid moieties (IS and IM) alternating with flexible PE-like sequences, which have a deep impact on barrier properties. The difference in mechanical and barrier properties for ISC10 and IMC10 films mainly depends on their crystal structures and crystallinity. The difference of crystallization ability between ISC10 and IMC10 can be

attributed to the chain orientation degree as shown in Figure 11, where A refers to the exo-links and B refers to the endo-links. It is obvious that ISC10 repetition unit contains three kinds of links: exo-endo (A-C10-B), exo-exo (A-C10-A) and endo-endo (B-C10-B), while IMC10 repetition unit contains only endo-endo (B-C10-B) links. As predicted by Chemdraw® Software, IMC10 has more regular bond connections in a short range that can crystallize, but the highly curved chains make it hard to crystallize by chain-chain packing. On the contrary, the exo-links in ISC10 induces a more oriented chain which can readily crystallize and give a more dense microstructure [73,74]: the more the exo-exo links are repeated in the chain the easier the chains crystallize by chain-chain packing. This difference in chain orientation explained why ISC10 showed better barrier properties.

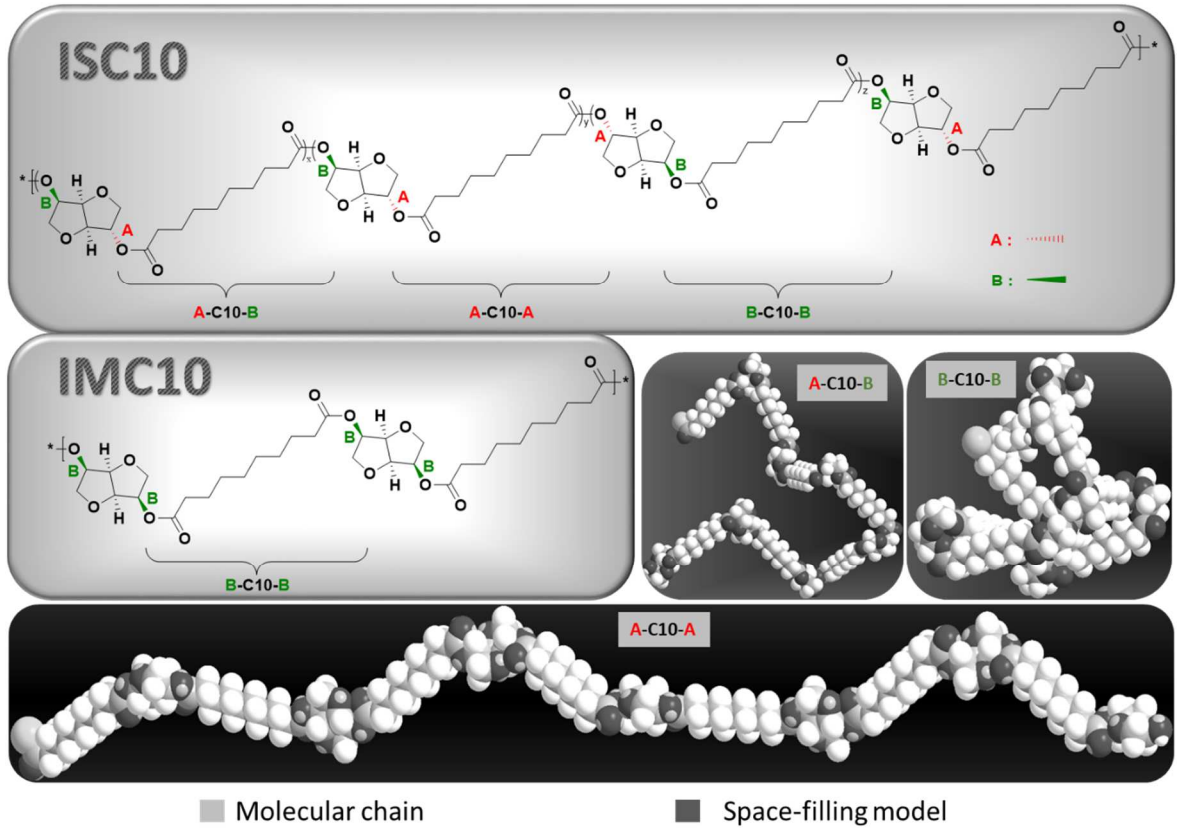

Figure 11 Polymer chains (gray) and the corresponding space-filling models (black) predicted by Chemdraw® Software

3 Conclusion

Six aliphatic bio-based polyesters including isosorbide and isomannide were successfully synthesized by bulk polycondensation. The chain length of the diacid units influenced the degradation and glass transition temperature as well as the crystallization. Only polyesters that contained more CH_2 repeat units (ISC10 and IMC10) showed good film forming properties. Crystallinity, with the presence of liquid crystal phase, was evidenced in both ISC10 and IMC10. The endo/exo stereoisomerism of isohexide units (IS or IM) slightly influenced the thermal degradation and glass transition temperature, but influenced the crystallization properties and then the mechanical and barrier properties. The exo-exo stereoscopic configurations in polyesters were more inclined to crystallize than the endo-endo configurations. Thus, polyesters prepared from isosorbide showed better tensile strength and better barrier properties to water and gases than isomannide polyesters. Furthermore, the ISC10 polyester showed more toughness and similar barrier properties for both water and gases compared to PLA, and was even more barrier to gases than the common food packaging material PE. Even if the barrier properties of ISC10 were lower than PET and PEF, the selectivity to CO_2 and O_2 was more favorable for fruits and vegetables preservation. Isosorbide polyesters showed more advantages over isomannide polyesters in terms of price and permeation properties. Ongoing studies are focused on increasing glass transition and melting temperatures as well as crystallinity to enhance the thermomechanical and barrier properties of these promising food packaging materials.

Acknowledgments

The authors thank Pr. S. Marais for POM observations, Dr. K. Fatyeyeva for water vapor permeation measurements, B. Jiang, C. Legrand and J. Bouillon for helpful discussions.

This manuscript is a tribute to the 50 year anniversary of the French Polymer Group (Groupe Français des Polymères - GFP).

Funding: This work was supported by the Chinese Scholarship Council [grant number 201701810120].

Data availability statement

The raw/processed data required to reproduce these findings cannot be shared at this time due to technical or time limitations.

References

[1] F. Carolyn, 2018, (2018). https://cleantechnica.com/demand-for-biodegradable-plastics-expected-to-surge/ics-expected-to-surge/.
[2] S. Farah, D.G. Anderson, R. Langer, Physical and mechanical properties of PLA, and their functions in widespread applications — A comprehensive review, Adv. Drug Deliv. Rev. 107 (2016) 367–392. https://doi.org/10.1016/j.addr.2016.06.012.
[3] E. Ten, L. Jiang, J. Zhang, M.P. Wolcott, Mechanical performance of polyhydroxyalkanoate (PHA)-based biocomposites, in: Biocomposites Des. Mech. Perform., Elsevier Inc., 2015: pp. 39–52. https://doi.org/10.1016/B978-1-78242-373-7.00008-1.
[4] C. Fang, X. Wang, X. Chen, Z. Wang, Mild synthesis of environment-friendly thermoplastic triblock copolymer elastomers through combination of ring-opening and RAFT polymerization, Polym. Chem. 10 (2019) 3610–3620. https://doi.org/10.1039/c9py00654k.
[5] S. Kobayashi, Green polymer chemistry: new methods of polymer synthesis using renewable starting materials, Struct. Chem. 28 (2017) 461–474. https://doi.org/10.1007/s11224-016-0861-3.
[6] C. Lavilla, A. Alla, A. Martínez de Ilarduya, S. Muñoz-Guerra, High Tg bio-based aliphatic polyesters from bicyclic-mannitol, Biomacromolecules. 14 (2013) 781–793. https://doi.org/10.1021/bm301854c.
[7] K.M. Zia, A. Noreen, M. Zuber, S. Tabasum, M. Mujahid, Recent developments and future prospects on bio-based polyesters derived from renewable resources: A review, Int. J. Biol. Macromol. 82 (2016) 1028–1040. https://doi.org/10.1016/j.ijbiomac.2015.10.040.
[8] H. Hu, R. Zhang, W. Bin Ying, L. Shi, C. Yao, Z. Kong, K. Wang, J. Wang, J. Zhu, Sustainable and rapidly degradable poly(butylene carbonate-co - cyclohexanedicarboxylate): Influence of composition on its crystallization, mechanical and barrier properties, Polym. Chem. 10 (2019) 1812–1822. https://doi.org/10.1039/c9py00083f.
[9] T. Kim, J.M. Koo, M.H. Ryu, H. Jeon, S.M. Kim, S.A. Park, D.X. Oh, J. Park, S.Y. Hwang, Sustainable terpolyester of high Tg based on bio heterocyclic monomer of dimethyl furan-2,5-dicarboxylate and isosorbide, Polymer. 132 (2017) 122–132. https://doi.org/10.1016/j.polymer.2017.10.052.
[10] Q. Ouyang, J. Liu, C. Li, L. Zheng, Y. Xiao, S. Wu, B. Zhang, A facile method to synthesize bio-based and biodegradable copolymers from furandicarboxylic acid and isosorbide with high molecular weights and excellent thermal and mechanical properties, Polym. Chem. 10 (2019) 5594–5601. https://doi.org/10.1039/c9py01314h.
[11] F. Fenouillot, A. Rousseau, G. Colomines, R. Saint-Loup, J.P. Pascault, Polymers from renewable 1,4:3,6-dianhydrohexitols (isosorbide, isomannide and isoidide): A review, Prog. Polym. Sci. 35 (2010) 578–622. https://doi.org/10.1016/j.progpolymsci.2009.10.001.
[12] J.A. Galbis, M.D.G. García-Martín, M.V. De Paz, E. Galbis, Synthetic polymers from sugar-based monomers, Chem. Rev. 116 (2016) 1600–1636. https://doi.org/10.1021/acs.chemrev.5b00242.
[13] F.H. Isikgor, Lignocellulosic Biomass: A sustainable platform for production of bio-based chemicals and polymers, Polym. Chem. 25 (2015) 4497–4559. https://doi.org/10.4324/9781315079097-35.
[14] A.F. Naves, H.T.C. Fernandes, A.P.S. Immich, L.H. Catalani, Enzymatic syntheses of unsaturated polyesters based on isosorbide and isomannide, J. Polym. Sci. Part A Polym. Chem. 51 (2013) 3881–3891. https://doi.org/10.1002/pola.26789.
[15] M. Rose, R. Palkovits, Isosorbide as a renewable platform chemical for versatile

applications-quo vadis?, ChemSusChem. 5 (2012) 167–176. https://doi.org/10.1002/cssc.201100580.

[16] A.L. Taylor, S. Ziesche, C. Yancy, P. Carson, R. D Agostino, K. Ferdinand, M. Taylor, K. Adams, M. Sabolinski, M. Worcel, J.N. Cohn, Combination of isosorbide dinitrate and hydralazine in blacks with heart failure, N. Engl. J. Med. 351 (2004) 2049-57. doi:10.1056/NEJMoa042934.

[17] J.N. Cohn, G. Johnson, S. Ziesche, F. Cobb, G. Francis, F. Tristani, R. Smith, W.B. Dunkman, H. Loeb, M. Wong, G. Bhat, S. Goldman, R.D. Fletcher, J. Doherty, C.V. Hughes, P. Carson, G. Cintron, R. Shabetai, C. Haakenson, A Comparison of enalapril with hydralazine–isosorbide dinitrate in the treatment of chronic congestive heart failure, N. Engl. J. Med. 325 (1991) 303-310. https://doi.org/10.1056/NEJM199108013250502.

[18] G. Cotter, E. Metzkor, E. Kaluski, Z. Faigenberg, R. Miller, A. Simovitz, O. Shaham, D. Marghitay, M. Koren, A. Blatt, Y. Moshkovitz, R. Zaidenstein, A. Golik, Randomised trial of high-dose isosorbide dinitrate plus low-dose furosemide versus high-dose furosemide plus low-dose isosorbide dinitrate in severe pulmonary oedema, Lancet. 351 (1998) 389-393. https://doi.org/10.1016/S0140-6736(97)08417-1.

[19] J. George, J.C. Prasana, S. Muthu, T.K. Kuruvilla, Spectroscopic (FT-IR, FT Raman) and quantum mechanical study on isosorbide mononitrate by density functional theory, Int. J. Mater. Sci. 12 (2017) 302-320.

[20] M.M. Redfield, et al. Isosorbide mononitrate in heart failure with preserved ejection fraction, N Engl J Med. 373 (2015) 2314-2338. https://doi.org/10.1056/NEJMoa1510774.

[21] G.W. Blair, J.P. Appleton, K. Flaherty, F. Doubal, N. Sprigg, R. Dooley, C. Richardson, I. Hamilton, Z.K. Law, Y. Shi, M.S. Stringer, M.J. Thrippleton, J. Boyd, K. Shuler, P.M. Bath, J.M. Wardlaw, Tolerability, safety and intermediary pharmacological effects of cilostazol and isosorbide mononitrate, alone and combined, in patients with lacunar ischaemic stroke: The LACunar Intervention-1 (LACI-1) trial, a randomised clinical trial, EClinicalMedicine. 11 (2019) 34-43. https://doi.org/10.1016/j.eclinm.2019.04.001.

[22] C. Dussenne, T. Delaunay, V. Wiatz, H. Wyart, I. Suisse, M. Sauthier, Synthesis of isosorbide: An overview of challenging reactions, Green Chem. 19 (2017) 5332-5344. https://doi.org/10.1039/c7gc01912b.

[23] D. Cao, B. Yu, S. Zhang, L. Cui, J. Zhang, W. Cai, Isosorbide production from sorbitol over porous zirconium phosphate catalyst, Appl. Catal. A Gen. 528 (2016) 59-66. https://doi.org/10.1016/j.apcata.2016.09.017.

[24] H. Kobayashi, H. Yokoyama, B. Feng, A. Fukuoka, Dehydration of sorbitol to isosorbide over H-beta zeolites with high Si/Al ratios, Green Chem. 17 (2015) 2732-2735. https://doi.org/10.1039/c5gc00319a.

[25] A. Yamaguchi, O. Sato, N. Mimura, M. Shirai, One-pot conversion of cellulose to isosorbide using supported metal catalysts and ion-exchange resin, Catal. Commun. 67 (2015) 59–63. https://doi.org/10.1016/j.catcom.2015.04.009.

[26] G. Flèche, M. Huchette, Isosorbide. Preparation, Properties and Chemistry, Starch - Stärke. 38 (1986) 26–30. https://doi.org/10.1002/star.19860380107.

[27] D.J. Saxon, A.M. Luke, H. Sajjad, W.B. Tolman, T.M. Reineke, Next-generation polymers: Isosorbide as a renewable alternative, Prog. Polym. Sci. 101 (2020) 101196. https://doi.org/10.1016/j.progpolymsci.2019.101196.

[28] X. Feng, A.J. East, W.B. Hammond, Y. Zhang, M. Jaffe, Overview of advances in sugar-based polymers, Polym. Adv. Technol. 22 (2011) 139-150.

https://doi.org/10.1002/pat.1859.
[29] D. Juais, A.F. Naves, C. Li, R.A. Gross, L.H. Catalani, Isosorbide polyesters from enzymatic catalysis, Macromolecules. 43 (2010) 10315-10319. https://doi.org/10.1021/ma1013176.
[30] J. Thiem, H. Lüders, Darstellung und gezielte polykondensation von anhydroalditol-bausteinen aus stärke, Starch - Stärke. 36 (1984) 170–176. https://doi.org/10.1002/star.19840360506.
[31] F. Aricò, P. Tundo, Isosorbide and dimethyl carbonate: A green match, Beilstein J. Org. Chem. 12 (2016) 2256–2266. https://doi.org/10.3762/bjoc.12.218.
[32] A.F. Sousa, A.C. Fonseca, A.C. Serra, C.S.R. Freire, A.J.D. Silvestre, J.F.J. Coelho, New unsaturated copolyesters based on 2,5-furandicarboxylic acid and their crosslinked derivatives, Polym. Chem. 7 (2016) 1049–1058. https://doi.org/10.1039/c5py01702e.
[33] J. Dai, S. Ma, N. Teng, X. Dai, X. Shen, S. Wang, X. Liu, J. Zhu, 2,5-Furandicarboxylic acid- and itaconic acid-derived fully biobased unsaturated polyesters and their cross-linked networks, Ind. Eng. Chem. Res. 56 (2017) 2650–2657. https://doi.org/10.1021/acs.iecr.7b00049.
[34] Y. Xu, G. Hua, M. Hakkarainen, K. Odelius, Isosorbide as core component for tailoring biobased unsaturated polyester thermosets for a wide structure-property window, Biomacromolecules. 19 (2018) 3077–3085. https://doi.org/10.1021/acs.biomac.8b00661.
[35] S. Ma, D.C. Webster, F. Jabeen, Hard and flexible, degradable thermosets from renewable bioresources with the assistance of water and ethanol, Macromolecules. 49 (2016) 3780–3788. https://doi.org/10.1021/acs.macromol.6b00594.
[36] Isosorbide polycarbonate: POLYSORB® bisphenol a alternative, isosorbide based polycarbonate. https://www.roquette.com/industries/performance-materials/polycarbonates. Accessed 25 May 2020.
[37] R. Tamion, F. Marsais, P. Ribereau, G. Queguiner, D. Abenhaim, A. Loupy, L. Munnier, Synthesis of new chiral auxiliaries derived from isosorbide, Tetrahedron: Asymmetry. 4 (1993) 1879–1890. https://doi.org/10.1016/S0957-4166(00)80428-0.
[38] D. Braun, M. Bergmann, 1,4:3,6-Dianhydrohexite als Bausteine für Polymere, J. Für Prakt. Chemie/Chemiker-Zeitung. 334 (1992) 298–310. https://doi.org/10.1002/prac.19923340403.
[39] C.J. Brandenburg, Process to produce polyesters which incorporate isosorbide, US 6,818,730 B2, 2004.
[40] M. Okada, K. Tsunoda, K. Tachikawa, K. Aoi, Biodegradable polymers based on renewable resources. IV. Enzymatic degradation of polyesters composed of 1,4:3.6-dianhydro-D-glucitol and aliphatic dicarboxylic acid moieties, J. Appl. Polym. Sci. 77 (2000) 338–346. https://doi.org/10.1002/(SICI)1097-4628(20000711)77:2<338::AID-APP9>3.0.CO;2-C.
[41] M. Okada, Y. Okada, A. Tao, K. Aoi, Biodegradable polymers based on renewable resources: Polyesters composed of 1,4 : 3,6-dianhydrohexitol and aliphatic dicarboxylic acid units, J. Appl. Polym. Sci. 62 (1996) 2257–2265. https://doi.org/10.1002/(SICI)1097-4628(19961226)62:13<2257::AID-APP10>3.0.CO;2-0.
[42] H.S. Park, M.S. Gong, J.C. Knowles, Synthesis and biocompatibility properties of polyester containing various diacid based on isosorbide, J. Biomater. Appl. 27 (2012) 99–109. https://doi.org/10.1177/0885328212447245.
[43] H. Marubayashi, T. Ushio, S. Nojima, Crystallization of polyesters composed of isohexides and aliphatic dicarboxylic acids: Effects of isohexide stereoisomerism and

dicarboxylic acid chain length, Polym. Degrad. Stab. 146 (2017) 174–183. https://doi.org/10.1016/j.polymdegradstab.2017.10.005.
[44] H. Marubayashi, T. Ushio, S. Nojima, Crystal Polymorphism of Biobased polyester composed of isomannide and succinic acid, Macromolecules. 52 (2019) 4624–4633. https://doi.org/10.1021/acs.macromol.8b02594.
[45] M. Schmid, W. Zillinger, K. Müller, S. Sängerlaub, Permeation of water vapour, nitrogen, oxygen and carbon dioxide through whey protein isolate based films and coatings-Permselectivity and activation energy, Food Packag. Shelf Life. 6 (2015) 21–29. https://doi.org/10.1016/j.fpsl.2015.08.002.
[46] Z. Hussein, O.J. Caleb, U.L. Opara, Perforation-mediated modified atmosphere packaging of fresh and minimally processed produce-A review, Food Packag. Shelf Life. 6 (2015) 7–20. https://doi.org/10.1016/j.fpsl.2015.08.003.
[47] D.K. Owens, R.C. Wendt, Estimation of the surface free energy of polymers, J. Appl. Polym. Sci. 13 (1969) 1741–1747. https://doi.org/10.1002/app.1969.070130815.
[48] S. Alix, S. Marais, C. Morvan, L. Lebrun, Biocomposite materials from flax plants: Preparation and properties, Compos. Part A Appl. Sci. Manuf. 39 (2008) 1793–1801. https://doi.org/10.1016/j.compositesa.2008.08.008.
[49] M. Métayer, M. Labbé, S. Marais, D. Langevin, C. Chappey, F. Dreux, M. Brainville, P. Belliard, Diffusion of water through various polymer films: A new high performance method of characterization, Polym. Test. 18 (1999) 533–549. https://doi.org/10.1016/S0142-9418(98)00052-X.
[50] C.L. Buquet, B. Ben Doudou, C. Chappey, E. Dargent, S. Marais, Permeation properties of poly(m-xylene adipamide) membranes, J. Phys. Chem. B. 113 (2009) 3445–3452. https://doi.org/10.1021/jp810241z.
[51] C. Joly, D. Le Cerf, C. Chappey, D. Langevin, G. Muller, Residual solvent effect on the permeation properties of fluorinated polyimide films, Sep. Purif. Technol. 16 (1999) 47–54. https://doi.org/10.1016/S1383-5866(98)00118-X.
[52] A.A. Morontsev, V.A. Zhigarev, R.Y. Nikiforov, N.A. Belov, M.L. Gringolts, E.S. Finkelshtein, Y.P. Yampolskii, A new approach to improvement of gas permeation properties of olefin metathesis derived poly(norbornenes): gem-difluorocyclopropanation of backbone double bonds, Eur. Polym. J. 99 (2018) 340–349. https://doi.org/10.1016/j.eurpolymj.2017.12.020.
[53] Q. Ding, D. Jehnichen, M. Göbel, M. Soccio, N. Lotti, D. Cavallo, R. Androsch, Smectic liquid crystal Schlieren texture in rapidly cooled poly(butylene naphthalate), Eur. Polym. J. 101 (2018) 90–95. https://doi.org/10.1016/j.eurpolymj.2018.02.010.
[54] J. Maiz, G. Liu, F. Ruipérez, N. Delbosc, O. Coulembier, D. Wang, A.J. Müller, How cyclic chain topology can reduce the crystallization rate of poly(3-hexylthiophene) and promote the formation of liquid crystalline phases in comparison with linear analogue chains, J. Mater. Chem. C. 7 (2019) 6548–6558. https://doi.org/10.1039/c9tc01609k.
[55] Q. Ding, M. Soccio, N. Lotti, N. Mahmood, D. Cavallo, R. Androsch, Crystallization of poly(butylene 2,6-naphthalate) containing diethylene 2,6-naphthalate constitutional defects, Polym. Cryst. 2 (2019). https://doi.org/10.1002/pcr2.10044.
[56] S. Farah, D.G. Anderson, R. Langer, Physical and mechanical properties of PLA, and their functions in widespread applications — A comprehensive review, Adv. Drug Deliv. Rev. 107 (2016) 367–392. https://doi.org/10.1016/j.addr.2016.06.012.
[57] J.Y. Kim, Y. Lee, D.Y. Lim, Plasma-modified polyethylene membrane as a separator for lithium-ion polymer battery, Electrochim. Acta. 54 (2009) 3714–3719. https://doi.org/10.1016/j.electacta.2009.01.055.
[58] S. Thanakkasaranee, D. Kim, J. Seo, Preparation and characterization of polypropylene/sodium propionate (PP/SP) composite films for bread packaging

application, Packag. Technol. Sci. 31 (2018) 221–231. https://doi.org/10.1002/pts.2369.
[59] K. Gotoh, A. Yasukawa, Y. Kobayashi, Wettability characteristics of poly(ethylene terephthalate) films treated by atmospheric pressure plasma and ultraviolet excimer light, Polym. J. 43 (2011) 545–551. https://doi.org/10.1038/pj.2011.20.
[60] E. Fortunati, F. Luzi, D. Puglia, F. Dominici, C. Santulli, J.M. Kenny, L. Torre, Investigation of thermo-mechanical, chemical and degradative properties of PLA-limonene films reinforced with cellulose nanocrystals extracted from Phormium tenax leaves, Eur. Polym. J. 56 (2014) 77–91. https://doi.org/10.1016/j.eurpolymj.2014.03.030.
[61] R.A. Auras, B. Harte, S. Selke, R. Hernandez, Mechanical, physical, and barrier properties of poly(lactide) films, J. Plast. Film Sheeting. 19 (2003) 123–135. https://doi.org/10.1177/8756087903039702.
[62] D. Cava, E. Giménez, R. Gavara, J.M. Lagaron, Comparative performance and barrier properties of biodegradable thermoplastics and nanobiocomposites versus PET for food packaging applications, J. Plast. Film Sheeting. 22 (2006) 265–274. https://doi.org/10.1177/8756087906071354.
[63] D.H. Weinkauf, D.R. Paul, Gas transport properties of thermotropic liquid-crystalline copolyesters. II. The effects of copolymer composition, J. Polym. Sci. Part B Polym. Phys. 30 (1992) 837–849. https://doi.org/10.1002/polb.1992.090300805.
[64] T. Kajiyama, Y. Nagata, E. Maemura, M. Takayanag, Molecular motion-permeability relationships in polycarbonate/liquid crystal (EBBA) composites membrane, Chem. Lett. (1979) 679–682.
[65] J. Hoshikawa, E. Seiko, K. Kabushiki, Liquid crystal display with barrier layer to reduce permeability, US Patent US4709991A, 1986.
[66] M.A. Ortenzi, L. Basilissi, H. Farina, G. Di Silvestro, L. Piergiovanni, E. Mascheroni, Evaluation of crystallinity and gas barrier properties of films obtained from PLA nanocomposites synthesized via “in situ” polymerization of L-lactide with silane-modified nanosilica and montmorillonite, Eur. Polym. J. 66 (2015) 478–491. https://doi.org/10.1016/j.eurpolymj.2015.03.006.
[67] M. Gholizadeh, J. Razavi, S.A. Mousavi, Gas permeability measurement in polyethylene and its copolymer films, Mater. Des. 28 (2007) 2528–2532. https://doi.org/10.1016/j.matdes.2006.09.018.
[68] N. Gontard, T. Labuza, Les emballages actifs, Tec et Doc, 2000.
[69] S.K. Burgess, G.B. Wenz, R.M. Kriegel, W.J. Koros, Penetrant transport in semicrystalline poly(ethylene furanoate), Polymer. 98 (2016) 305–310. https://doi.org/10.1016/j.polymer.2016.06.046.
[70] P.M. Budd, N.B. McKeown, Highly permeable polymers for gas separation membranes, Polym. Chem. 1 (2010) 63–68. https://doi.org/10.1039/b9py00319c.
[71] B. Bideau, J. Bras, N. Adoui, E. Loranger, C. Daneault, Polypyrrole/nanocellulose composite for food preservation: Barrier and antioxidant characterization, Food Packag. Shelf Life. 12 (2017) 1–8. https://doi.org/10.1016/j.fpsl.2017.01.007.
[72] L. Genovese, M. Soccio, N. Lotti, M. Gazzano, V. Siracusa, E. Salatelli, F. Balestra, A. Munari, Design of biobased PLLA triblock copolymers for sustainable food packaging: Thermo-mechanical properties, gas barrier ability and compostability, Eur. Polym. J. 95 (2017) 289–303. https://doi.org/10.1016/j.eurpolymj.2017.08.001.
[73] V. Morillon, F. Debeaufort, G. Blond, M. Capelle, A. Voilley, Factors affecting the moisture permeability of lipid-based edible films: A review, Crit. Rev. Food Sci. Nutr. 42 (2002) 67–89. https://doi.org/10.1080/10408690290825466.
[74] Q. Liu, X. Sun, H. Li, S. Yan, Orientation-induced crystallization of isotactic

polypropylene, Polymer. 54 (2013) 4404–4421. https://doi.org/10.1016/j.polymer.2013.04.066.

Graphical abstract